ADVANCED HEALTHCARE MATERIALS
www.advhealthmat.de

3D-Printed Hydrogel-Filled Microneedle Arrays

*Lindsay Barnum, Jacob Quint, Hossein Derakhshandeh, Mohamadmahdi Samandari, Fariba Aghabaglou, Ali Farzin, Laleh Abbasi, Sidi Bencherif, Adnan Memic, Pooria Mostafalu, and Ali Tamayol**

Microneedle arrays (MNAs) have been used for decades to deliver drugs transdermally and avoid the obstacles of other delivery routes. Hydrogels are another popular method for delivering therapeutics because they provide tunable, controlled release of their encapsulated payload. However, hydrogels are not strong or stiff, and cannot be formed into constructs that penetrate the skin. Accordingly, it has so far been impossible to combine the transdermal delivery route provided by MNAs with the therapeutic encapsulation potential of hydrogels. To address this challenge, a low cost and simple, but robust, strategy employing MNAs is developed. These MNAs are formed from a rigid outer layer, 3D printed onto a conformal backing, and filled with drug-eluting hydrogels. Microneedles of different lengths are fabricated on a single patch, facilitating the delivery of various agents to different tissue depths. In addition to spatial distribution, temporal release kinetics can be controlled by changing the hydrogel composition or the needles' geometry. As a proof-of-concept, MNAs are used for the delivery of vascular endothelial growth factor (VEGF). Application of the rigid, resin-based outer layer allows the use of hydrogels regardless of their mechanical properties and makes these multicomponent MNAs suitable for a range of drug delivery applications.

1. Introduction

Microneedle arrays (MNAs) are patches of microscale needles that can painlessly pass through the stratum corneum to reach the epidermis and facilitate the delivery of therapeutics in various medical contexts. MNAs used for drug delivery are typically found in four forms:[1] solid MNAs, which increase drug permeation by puncturing the skin,[2] hollow MNAs that deliver a drug solution directly past the skin,[3] polymer-based MNAs that release an encapsulated drug upon dissolving in the skin,[4] and MNAs that release a loaded drug from a dissolving coating.[5] MNAs have been manufactured using a range of materials, such as silicon,[6] ceramics[7] and glass,[8] metals,[9] and polymers,[10] and methods including micromolding,[11] laser cutting,[12] etching,[13] drawing lithography,[14] and microinjection.[15] Through selection of the correct combination of material and technique, a wide array of needle geometries, from hypodermic style[16] to flat sheet metal needles[17] to complex structures with reverse facing barbs for tissue adhesion,[18] can be realized. This robust technology has been developed and studied for years for biomedical applications ranging from combined chemo-photothermal skin cancer treatment[19] to blood glucose monitoring[20] to continuous contraceptive delivery.[21]

L. Barnum, J. Quint, H. Derakhshandeh, Dr. M. Samandari, Dr. F. Aghabaglou, Dr. L. Abbasi, Prof. A. Memic, Prof. A. Tamayol[+]
Department of Mechanical and Materials Engineering
University of Nebraska
Lincoln, NE 68588, USA
E-mail: atamayol@uchc.edu

Dr. A. Farzin[++], Dr. P. Mostafalu
Department of Medicine
Brigham and Women's Hospital
Harvard Medical School
Boston, MA 02139, USA

The ORCID identification number(s) for the author(s) of this article can be found under https://doi.org/10.1002/adhm.202001922

[+]Present address: Department of Biomedical Engineering, University of Connecticut Health Center, Farmington, CT 06030, USA

[++]Present address: Department of Tissue Engineering and Applied Cell Sciences, School of Advanced Technologies in Medicine, Tehran University of Medical Sciences, Tehran, Iran

DOI: 10.1002/adhm.202001922

Prof. S. Bencherif
Department of Chemical Engineering
Department of Bioengineering
Northeastern University
Boston, MA 02115, USA

Prof. S. Bencherif
John A. Paulson School of Engineering and Applied Sciences
Harvard University
Cambridge, MA 02128, USA

Prof. A. Memic
Center of Nanotechnology
King Abdulaziz University
Jeddah 21589, Saudi Arabia

Among the many materials used in biomedical engineering, hydrogels have drawn significant attention due to their amenable and controllable physical and mechanical characteristics. In various tissue engineering contexts, a major application of hydrogels has long been in their use in the encapsulation and subsequent release of bioactive molecules.[22] Their naturally highly porous network of hydrophilic chains with high water content[23] allows hydrogels to carry aqueous solutions of hydrophilic compounds, which slowly diffuse out into the surrounding environment.[24] Since hydrogels can be engineered with tunable degradation profiles, they offer controlled release options for long-term delivery of therapeutics. In addition, molecules can be conjugated to their polymer backbone chemically or electrostatically in order to modulate their release kinetics.[25] A class of "smart" hydrogels that can react to environmental stimuli, such as changes in pH or local concentration of certain biomolecules, are also an ongoing subject of interest for highly specific drug targeting.[26] Active release constructs that can be externally triggered, such as those developed for wound care,[27] can overcome off-target stimulation of smart materials that may release molecules prematurely or in response to environmental noise. However, another key drawback cited for these smart hydrogels is their low strength and stiffness, especially since these constructs often need to be small or thin, as large systems suffer from slow stimulus response.[26]

This has been a problem in the translation of hydrogels into usable MNAs, as hydrogels in their hydrated form are typically too weak to penetrate human skin and other tissues. This is a particularly fundamental challenge for applications where longer needles are needed; for example, for the treatment of chronic wounds, where the MNAs should be long enough to penetrate through surface layers of tissue and biofilm. Traditional hypodermic needles have been utilized to inject hydrogels for sustained drug delivery in wound care treatments,[28] but this technique lacks spatial control and does not allow for removal of the gel in the case of allergic or immunogenic reaction. To address this, hydrogel MNAs have been developed that can pierce the skin, utilizing a tough polymer coating that eventually degrades to reveal the gel core,[29] or dehydration of the gels, which dissolve in situ.[30] While these hydrogel-based needles provide improved spatial distribution of therapeutics, they are too brittle to be successfully retracted when necessary, and are therefore designed to be left in place after application.

Additionally, while existing MNAs improve upon hydrogel injection in terms of increased surface spatial control of release, they have not typically been designed to target different therapeutics to different areas of tissue, nor have they been structured to reach multiple tissue depths. Controlling 3D spatial distribution is essential in the delivery of drugs and biological factors. For example, some biological processes, such as vascularization and angiogenesis, can be guided and expedited in the presence of a gradient of angiogenic factors. Utilization of 3D printing to create polymer-based MNAs has drawn growing interest recently, and these technologies may hold the solution to individualized control of drug delivery.[18,31] 3D printing technology has been shown to allow complete customization of an MNA's geometry, including both array properties such as total size and needle density, and individual needle characteristics such as shape and length.[32] Additionally, more complex geometries can be realized with 3D printing than traditional fabrication methods while also offering rapid flexibility in design. By harnessing the power of 3D printing in combination with a polymer shell/hydrogel core design, in this manuscript, we have developed a strategy that collectively addresses the above-mentioned challenges.

A 3D printing manufacturing method allowed us to simply and rapidly create a hollow multilength MNA design. The polymer shell facilitated smooth insertion into skin while protecting the hydrogel contained within. Compression and penetration testing confirmed that, unlike previous core and shell MNA systems, this patch is robust enough to be easily removed in case of an allergic or otherwise negative reaction. Release studies demonstrated the controlled release capability of the hydrogel cores, showing similar release profiles from multiple gels. In addition, the multilength design promoted delivery of different therapeutics to different layers of tissue, demonstrated through a dual release study into a gel skin model. Finally, a scratch assay exhibited the MNA's ability to encapsulate and subsequently deliver vascular endothelial growth factor (VEGF) as a model bioactive growth factor. This MNA is a powerful tool that facilitates intradermal delivery of therapeutics from materials that would not otherwise be strong enough to pierce the skin.

2. Results and Discussion

In addition to the potential for transdermal delivery of drugs for systemic administration from MNAs, there are many skin injuries and disorders that could benefit from transdermal delivery of therapeutics. For example, in chronic wounds, where healing is impaired, it has been shown that the delivery of drugs and biological factors can boost physiological healing processes, but their efficacy is dependent on the delivery method.[31c,33] Since, upon injury, the skin barrier is breached, it has been believed that the topical delivery of drugs would allow their proper penetration and distribution. However, the formed eschar, a crust of necrotic tissue that dries and hardens postinjury,[34] combined with exudate flow rich with various enzymes can lower the bioavailability of topically delivered compounds to the target cells. It has recently been shown that the intradermal delivery of therapeutics is superior to topically delivery for improving diabetic wound healing,[31c] and there is growing interest in the use of MNAs to treat these kinds of wounds.[35] Additionally, it is well known that the release kinetics of drugs and bioactive factors affect their effectiveness. Indeed, spatiotemporal control has been identified as an essential characteristic of effective bioactive factor delivery systems.[33] Therefore, it is expected that controlling the spatiotemporal distribution of various biological factors and drugs will improve the healing rate of chronic wounds and other skin conditions.

Over the course of this study, we developed a strategy that enabled the spatiotemporal control of delivered drugs to different layers of the skin. The platform is composed of MNAs with different needle lengths, in which each individual needle can be loaded independently. A schematic illustrating the developed platform is shown in **Figure 1**a, demonstrating that by encapsulating drugs in different hydrogels integrated within these needles, the release kinetics of each drug can be customized. Furthermore, it is illustrated how needles of different lengths enable a spatially controlled distribution of drugs across the depth of the skin tissue. For ease of in-lab manipulation in this proof-of-concept study, we

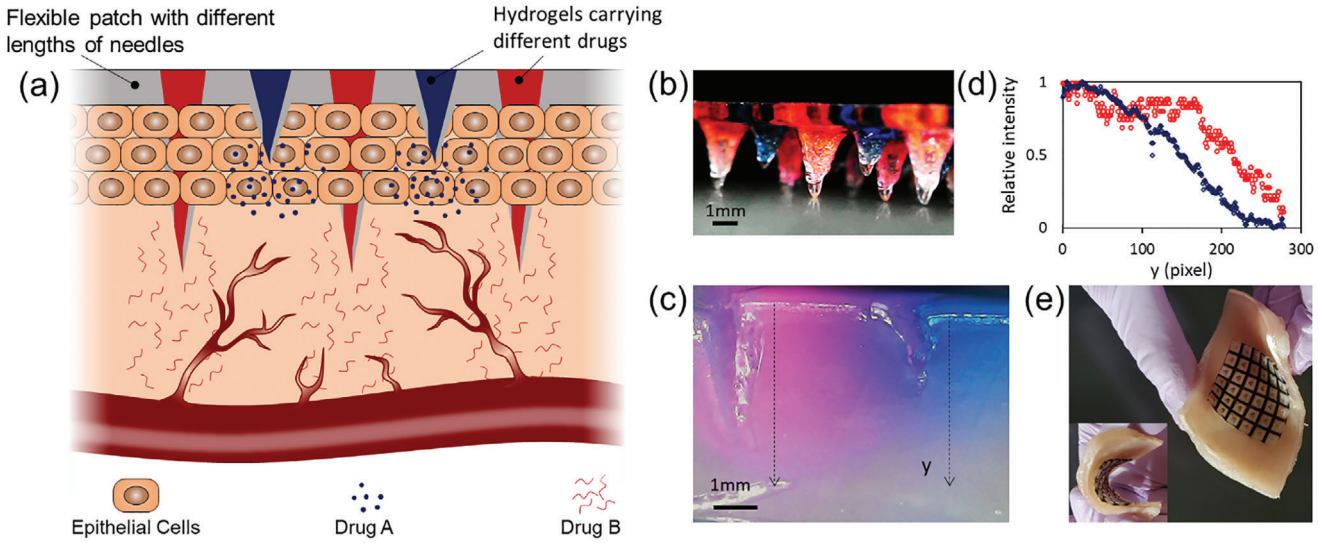

Figure 1. The use of miniaturized needle arrays (MNAs) for enhancing the bioavailability of drugs at the desired tissue depths. a) Schematic representation of the MNA-based dressing for the delivery of two different therapeutics targeting different depths or regions of the tissue to target separate cell populations. b) A typical 3D-printed multilength needle array, in which the needles of different lengths were filled with hydrogels carrying different agents (shown here with different colors). c) The qualitative and d) quantitative distribution of different dyes in an agarose skin model released from the multilength MNA bandage. The intensity is graphed along the lines indicated in panel (c). e) Compliance of the semiflexible MNA on a sample of pig skin.

used utilized 2 and 3 mm needles to demonstrate the trends in release depth and kinetics. These needle lengths have the potential to be painful during application; however, these values are tunable and could be shortened for in vivo use. Depending on the location on the body, the human epidermis can vary in thickness from 0.1 to 1.5 mm,[36] and the dermis can range from <1 to 5 mm,[37] so the needle lengths can be adjusted to meet the needs of the skin at the administration site. The MNAs could also be coated with an anesthetic as needed. Additionally, there are a number of applications where patients have experienced nerve destruction, including severe burns and neuropathic diabetic chronic wounds, and could benefit from the controlled intradermal drug delivery without risk of pain. Animal work has also been done with needles of a similar length and shown success at improving wound healing.[38] In the case of a chronic wound application, the shorter needles would target the epidermis while longer needles could penetrate into the dermis and release their payload into these deeper layers. As an example, longer needles could be loaded with VEGF-containing hydrogels to deliver these biochemical cues to the existing vasculature in the dermis. VEGF, a well-established proangiogenic factor, can enhance angiogenesis in the wound bed,[39] resulting in enhanced perfusion of nutrients and oxygen while allowing the infiltration of immune and stem cells to the wound bed, and ultimately facilitating tissue repair that had been hindered by lack of VEGF.[40] Antibiotics, on the other hand, could be loaded into the shorter needles and be delivered specifically to the necrotic tissue typically colonized with pathogens. This would lead to the elimination of infection without interrupting the healing process due to adverse antibiotic effects.[41] A representative picture of a typical dressing with two different needle lengths, in which each group carries a different dye, is shown in Figure 1b; the details of the fabrication of gel-filled needles are provided in the "Experimental Section." Upon insertion into an agarose gel, the hydrogels embedded inside the needles began to release their cargo. The spatial distribution of different dyes within the agarose gel is demonstrated (Figure 1c). As expected, longer needles can increase the bioavailability of drugs in the deeper layers of the skin-mimicking gel, while the payload in the shorter needles is concentrated closer to the surface (Figure 1d). The final MNA design was composed of rigid resin needles and islands that held together with a more compliant, rubber-like material, providing both stability for insertion and flexibility to conform to topographical skin surfaces (Figure 1e).

MNAs have been fabricated using a wide variety of materials and different strategies such as micromolding, laser ablation, drawing, and photolithography.[11] While these microfabrication approaches offer good structural resolution, they rely on expensive facilities; their flexibility is limited; and/or they have a low throughput.[22a] Also, while they can be used to fabricate small-scale structures, typically fabrication of these structures with multiple heights is not feasible. Recent advancements in 3D printing have improved resolution, reduced costs, and increased throughput.[42] Also inherent to the 3D printing technique is the ability to fabricate complex structures, such as multiheight MNAs. Recently, micro- and miniaturized needles have been fabricated using 3D printing, and their benefits for the treatment of a number of diseases have been demonstrated.[31b,c]

A limitation of using hydrogels to fabricate MNAs is their poor mechanical properties for forming high-aspect-ratio structures capable of penetrating the skin. To overcome this challenge, we have developed bilayered MNAs in which the exterior was formed from a rigid biocompatible resin, and the interior was filled with hydrogels carrying biologically relevant agents.

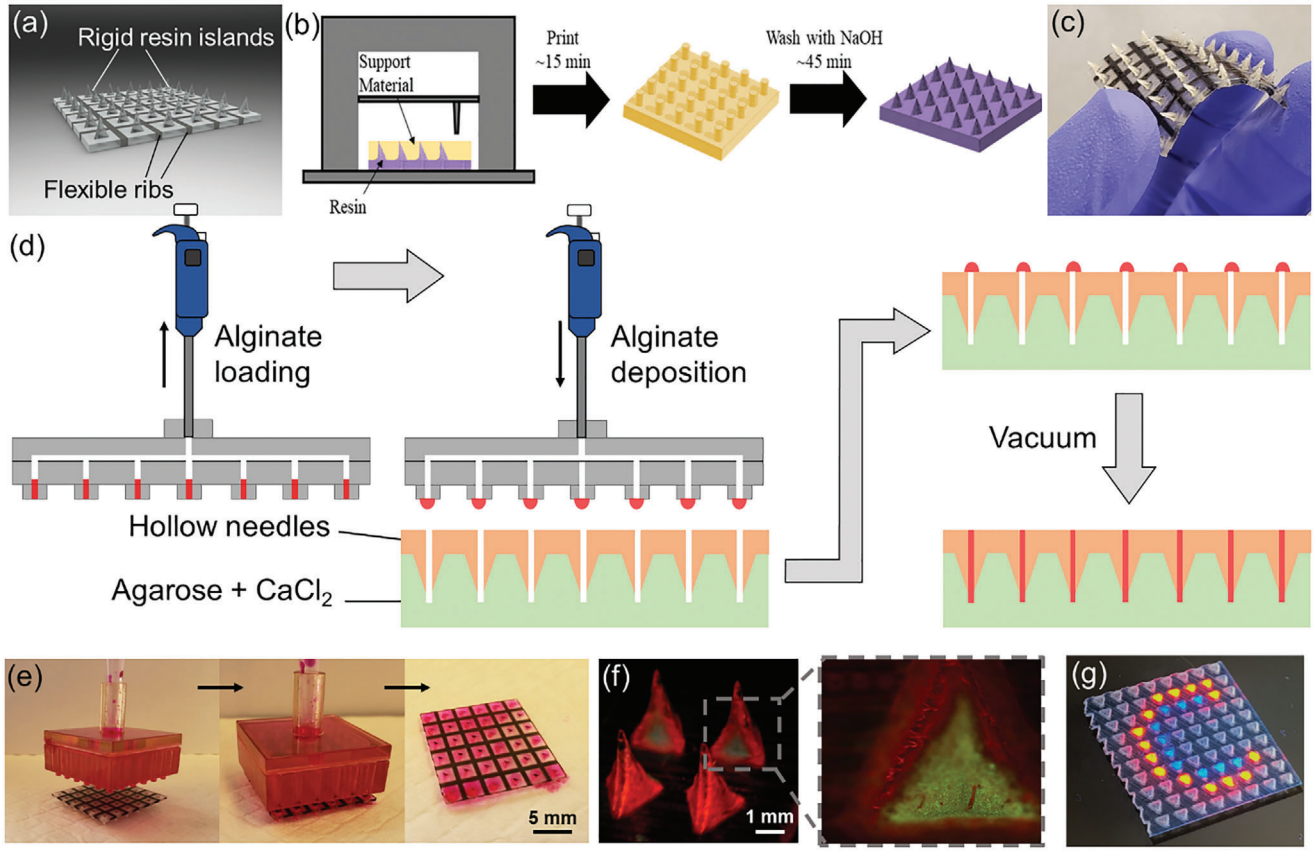

Figure 2. MNA fabrication and gel filling. a) SolidWorks design of semiflexible MNA. b) Schematic illustration of the fabrication process using 3D printing followed by cleaning with NaOH to remove support material. c) Actual demonstration of semiflexible MNAs. d) Concept drawing of loading mechanism for filling MNAs. e) Demonstration of rhodamine dyed alginate deposition using the loading mechanism. f) Fluorescent imaging of filled needles. g) Proof of concept illustrating spatial control over individual needles. Two "C"-shaped patterns in the array were filled with gels containing red and blue dyes, while the rest were filled with a transparent gel.

In the current study, we tested alginate and poly(ethylene glycol diacrylate) (PEGDA) as two examples of ionically and covalently crosslinkable hydrogels, respectively.

The designed MNAs (**Figure 2**a) were printed using a material jetting (MJ) 3D printer, and then the support material was removed using a NaOH solution to expose the resin construct underneath (Figure 2b). The printer that was used can print objects with a combination of materials. This capability allows for the fabrication of MNAs with a tunable degree of flexibility using rigid needles connected by flexible and rubber-like ribs (Figure 2c). The semiflexible dressing maintained appropriate needle rigidity and orientation during insertion while providing flexibility to conform to curved body surfaces or uneven wound topography (Figure 2c).

To facilitate and enhance the reproducibility and controllability of the filling process, we created a loading mechanism that can fill the entire MNA at once or a designated section, a concept that is easy to scale up and automate. During the needle-loading process (Figure 2d), the array was inserted into an agarose gel containing calcium chloride ($CaCl_2$). The attachment was loaded with an alginate prepolymer through normal pipette operation, with fluid flowing into all of the channels. The prepolymer could then be precisely deposited over each needle on an array. The array was placed in a vacuum chamber to force the prepolymer to flow into the needles, where it contacted the agarose and was crosslinked by the calcium ions contained therein. Additional $CaCl_2$ solution was pipetted over the backs of the needles to ensure complete crosslinking.

This mechanism is designed to fit on a P200 micropipette and has 36 conical channels with dimensions to match the semiflexible MNAs. It was tested with a 1% alginate solution mixed with rhodamine B (Rh-B) for better visualization. The prepolymer was easily pulled into the attachment channels and deposited over the needle openings on the MNA (Figure 2e).

To show the space occupied by the hydrogel, the resin shells of an MNA were stained with Rh-B and then filled with alginate hydrogel containing fluorescein isothiocyanate (FITC). The MNAs were imaged using a fluorescent microscope (Figure 2f). Each needle consists of a hollow triangular pyramid with one side open and exposed to allow the contained hydrogel to interface with the tissue environment, which allows diffusion of the therapeutic molecules. The large surface area facilitates controlled release through diffusion, while the structure of the needle keeps the hydrogel contained, and therefore, removable. Unlike an injection delivery method, a removable patch allows for easy withdrawal in the case of any adverse reaction to the incorporated compounds,

or in response to a change in the wound environment. One important benefit of the proposed fabrication approach is the ability to control over the spatial distribution of the loaded therapeutics. In this case, by using predesigned loading systems, the planar distribution of drugs within the patch can be controlled. Figure 2g shows a typical patch in which two "C"-shaped patterns of needles were formed with blue- and red-colored gels within an array filled with transparent gels.

The mechanical properties of the MNAs were evaluated to ensure they were mechanically robust enough that they did not sustain any damage upon insertion into a wound (**Figure 3**). Compressive force was applied to the needles up to and past their failure point, up to 200 N (Figure 3a). The 2 mm long MNAs failed at ≈12% strain of jaw displacement, while the larger 3 mm long failed at about 16% strain. This failure is characterized by a plateau in the force–displacement curve where the applied force is not increasing but the displacement of the upper jaw continues (Figure 3b). MNAs failed via bending rather than being shattered, crushed, or snapped off of the substrate (Figure 3c). It is important that if the needles fail due to excessive force, they bend rather than break off into the wound bed, which could aggravate the local inflammation. Overall, compression testing was performed to a much greater maximum force than it actually takes to insert these needles into the skin.

Next, we performed insertion testing using a pig skin model (Figure 3d). The tests were conducted with nonflexible, flexible, and semiflexible arrays. Nonflexible arrays were entirely fabricated from the rigid resin, while in the fully flexible design, the backing was entirely made of a rubber-like material. In the semiflexible design, however, a single needle and its backing within the array were separated by narrow ribs of rubber-like material. As shown in Figure 3e, the fully flexible arrays could not penetrate the pig skin. The low increase in force in the curve shown in Figure 3e resulted from the needles bending out of plane due to deformation of the backing. As a result, the array was not stiff enough to penetrate the pig skin. The nonflexible arrays functioned as intended with the rigid backing holding the needles in place and not deforming as they successfully penetrated the pig skin. However, rigid backing cannot make conformal contact with skin or a wound surface. The semiflexible arrays followed a very similar force trace, suggesting that the incorporation of flexible ribs makes them conformal to the skin without affecting their ease of penetration.

The gel-filled MNAs were inspected before and after penetration into pig skin to ensure that the hydrogel would not be pulled out of the needles during removal from a wound. The images from a typical MNA, filled with a colored gel for better visualization, before and after insertion into pig skin are shown in Figure 3f. It can be seen that the gel remained intact during needle insertion and after retraction. We do not expect the alginate to dissociate rapidly in the wound bed as the rate of ion exchange is typically slow.

As previously discussed, the spatial distribution of delivered drugs could be controlled within the engineered patch. For example, different rows of needles were filled with gels containing either Rh-B (red) or FITC (green). The needles were then inserted into pig skin and left on the skin for several minutes. Upon needle removal, the spatial distribution of colors within the pig skin can be seen (Figure 3g). To verify that the MNA was capable of penetrating both the epidermis and dermis, an MNA was inserted into a sample of pig skin, and hematoxylin and eosion (H&E) staining was performed (Figure 3h). The holes left by the needles can be clearly seen passing through the epidermis and into the dermis of the sample.

The hydrogel embedded within the MNAs was examined by scanning electron microscopy (SEM; **Figure 4**a). To capture the internal microstructure, needles were overfilled with 1% alginate, lyophilized, and the gels were broken to expose their cross section. The image also shows the gel–resin interface, highlighting the adhesion of the gel to the resin. This adhesion is crucial to ensure that when MNAs are removed from the skin, the gel remains within the needles rather than being pulled out. Higher magnification of the internal structure demonstrated the porous nature of the alginate hydrogel formed inside the needles (Figure 4b). The porosity of hydrogels is integral to their ability to contain and deliver molecules, and the pore size can affect the release kinetics.[25] Alginate crosslinked into a network of connected pores of similar size, essentially functioning like a sponge to store and release the loaded biologics.[43]

Confinement of the gel within the rigid needle structure enables easy removal of the MNA and provides the opportunity to replace it as needed. This could be necessary for transdermal delivery of therapeutics in case of an allergic or immunogenic reaction from the patient. This would also be valuable for wound treatment, because in this dynamic environment, drugs or growth factors that improve wound conditions at one stage of healing may be useless or harmful during a different stage. The platform developed addresses these rapidly changing conditions since it can be quickly and easily replaced with another MNA loaded with new therapeutics that are most relevant at a given phase of the wound healing process. Additionally, it is clinically recommended to replace dressings every 2–3 days to prevent infection.[44] This time frame was used as a basis for determining the desired period of release from the hydrogels cores. A number of release studies were conducted to determine delivery kinetics under several different conditions. The effect of hydrogel composition, molecular size of the encapsulated drugs, and needle geometry on the release kinetics was evaluated.

Rh-B was considered as a low-molecular-weight drug model, and its release from alginate embedded in the MNAs was assessed using various needle geometries and alginate compositions (Figure 4c,d). First, 3 mm long needles were filled with 1%, 2%, and 3% (w/v) alginate containing Rh-B to explore the effect of concentration (Figure 4c). As expected, the release rate was higher initially and decreased after 6 h. These results suggested that increasing the alginate concentration could decrease the release rate of Rh-B. A similar experiment was performed with 2 mm long needles containing the same alginate gels (Figure 4d). The release profile of Rh-B from the 2 mm long MNAs was overall similar to the longer needles. However, the total amount of released Rh-B decreased compared to experiments with 3 mm long needles, which was attributed to the decreased available volume of the hydrogel in the smaller needles. In both experiments, the 1% alginate released more than the 2% and 3% alginate groups, demonstrating the ability to tailor the releas kinetics with hydrogel composition and pore size. Representative SEM images showing the varied pore sizes of 1%, 2%, and 3% alginate are presented in Figure S8 (Supporting Information).

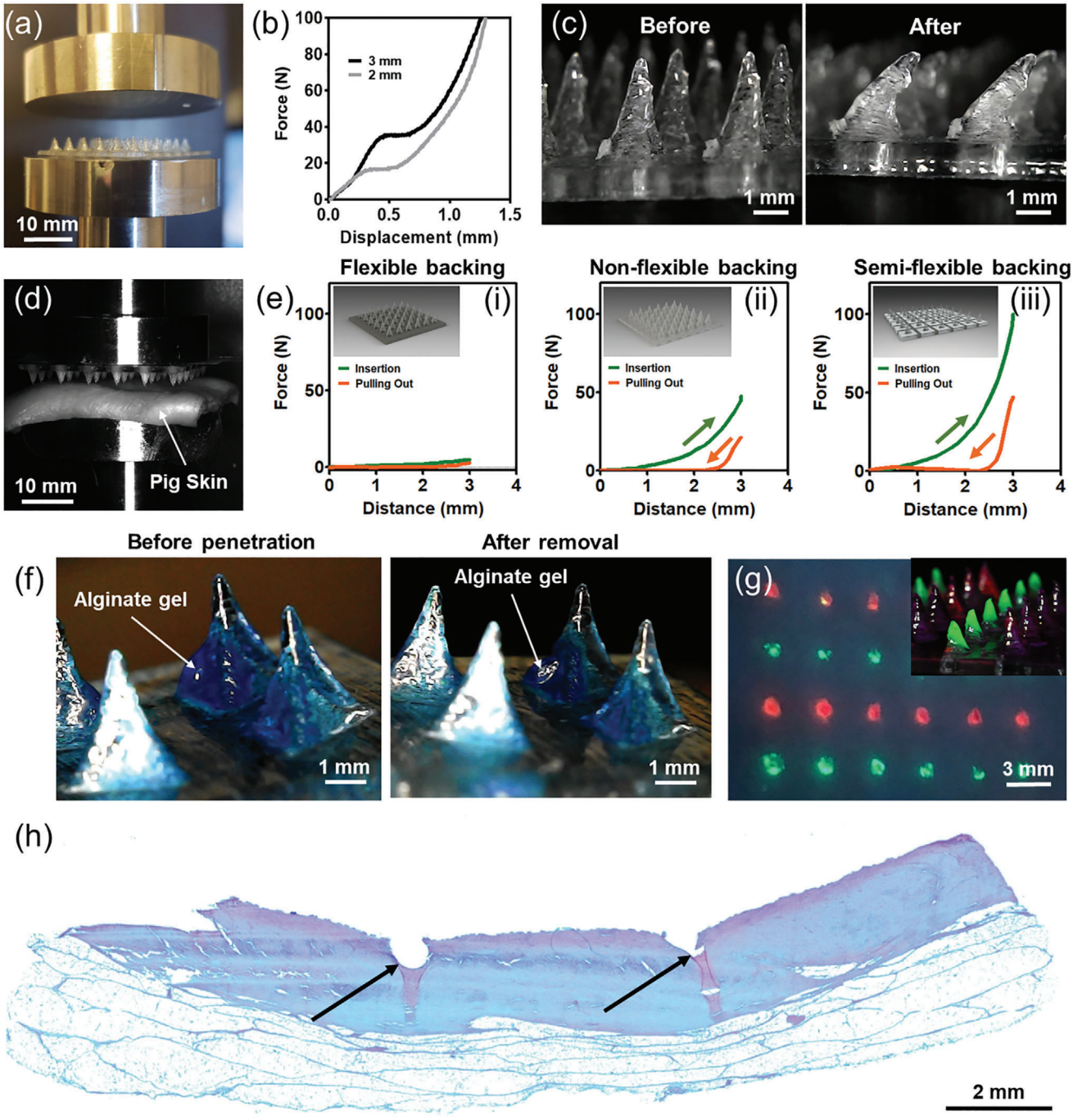

Figure 3. Mechanical properties and penetration testing. a) Setup employed for the mechanical testing of MNAs. b) Force–displacement curves obtained from the compression testing of 2 and 3 mm long MNAs. c) Needle morphology before and after the compression testing. The needles bent under compression demonstrating the desired failure mechanism. d) Pig skin insertion testing configuration. e) Representative force–displacement curves for pig skin insertion tests on MNAs with i) completely flexible backing, ii) nonflexible backing, and iii) semiflexible backing. f) Embedded alginate hydrogel in needles before and after insertion into pig skin. g) Pig skin after insertion of multilength MNA with 3 mm needles labeled with Rh-B (red) and 2 mm needles labeled with FITC (green). h) H&E staining of pig skin section that was penetrated with MNA. Black arrows indicate where needles pierced the skin.

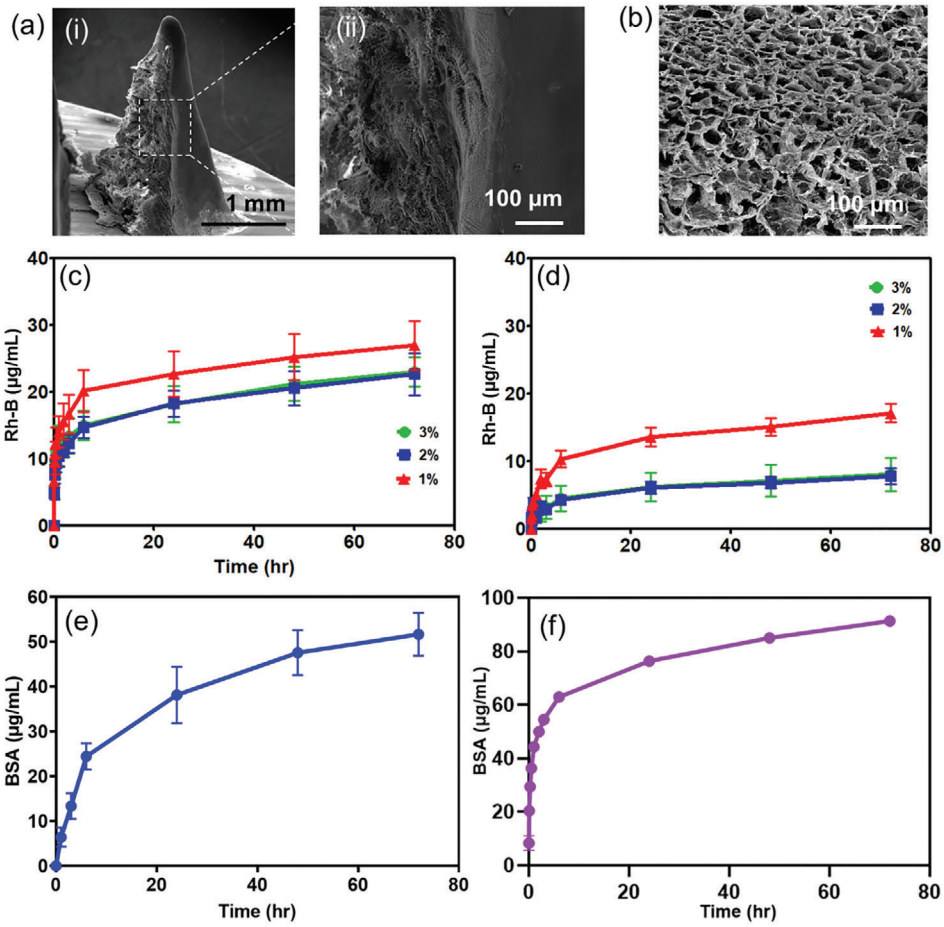

Figure 4. Microstructure and drug delivery characterization of hydrogels embedded in MNAs. a-i,ii) SEM images of resin/alginate interface in filled needles with different magnification levels. b) SEM image of the 1% alginate microstructure demonstrating its natural porous network. Release kinetics of Rh-B as a small-molecule drug model from different concentrations of alginate embedded in MNAs with c) 3 mm, or d) 2 mm needles. Release profile of BSA as a protein resembling growth factors from e) alginate and f) PEGDA, embedded in 3 mm needles. Error bars for panel (f) are too small to be seen after the 0 h time point, but standard deviation values are provided in Table S1 (Supporting Information).

To test the versatility of the platform, the delivery of bovine serum albumin (BSA), used as a model protein, was evaluated (Figure 4e,f). The delivery of proteins such as growth factors has been widely used to enhance wound healing.[45] BSA release from 1% (w/v) alginate was slower in comparison to Rh-B, especially in the initial hours, which could be due to the larger molecular size of the BSA and/or a higher affinity of BSA to the alginate (Figure 4e).[46]

The compatibility of the platform with another hydrogel was examined through the application of PEGDA as a photocrosslinkable hydrogel. The release of BSA from PEGDA hydrogels was faster than that in alginate hydrogels (Figure 4f), most likely due to the difference between the network electrostatic charges. These findings indicate that the composition of the hydrogel, potentially the network electrostatic charge, as well as the geometrical features of the needles can be optimized to fine-tune controlled drug delivery. However, the fabrication of gels from PEGDA was more challenging due to limited penetration of light into the needles. As a result, ensuring the reproducibility of the exact volume of the crosslinked gel within the needles might be difficult.

Correct dosage is vital in the drug delivery; an insufficient amount will be ineffective, and an excessive dose can cause local and systemic side effects and toxicity. The developed MNA allows different methods for controlling the amount of delivered therapeutic. First, the drug concentration in the hydrogels can be easily adjusted before loading, which determines the total drug mass contained in the MNA. Additionally, the geometry of the array can be customized in terms of needle density, total needle count, and needle size, all of which can be used to control the total volume of hydrogel that will be exposed to the tissue. In this way, the total drug dose can also be controlled. Finally, optimizing a hydrogel delivery profile for a particular drug gives precise control of the drug delivered over time, so the dose is continuously maintained in the effective therapeutic range.

An additional release experiment was conducted to evaluate the performance of the MNA at the dual delivery of drugs. An alternate design (Figure S6, Supporting Information) employing a wall along the base of the longer needle was utilized to improve drug localization to the desired depth. For this release, alginate mixed with Rh-B was loaded into the longer needles, with BSA FITC conjugate (BSA–FITC)-laden alginate in the shorter

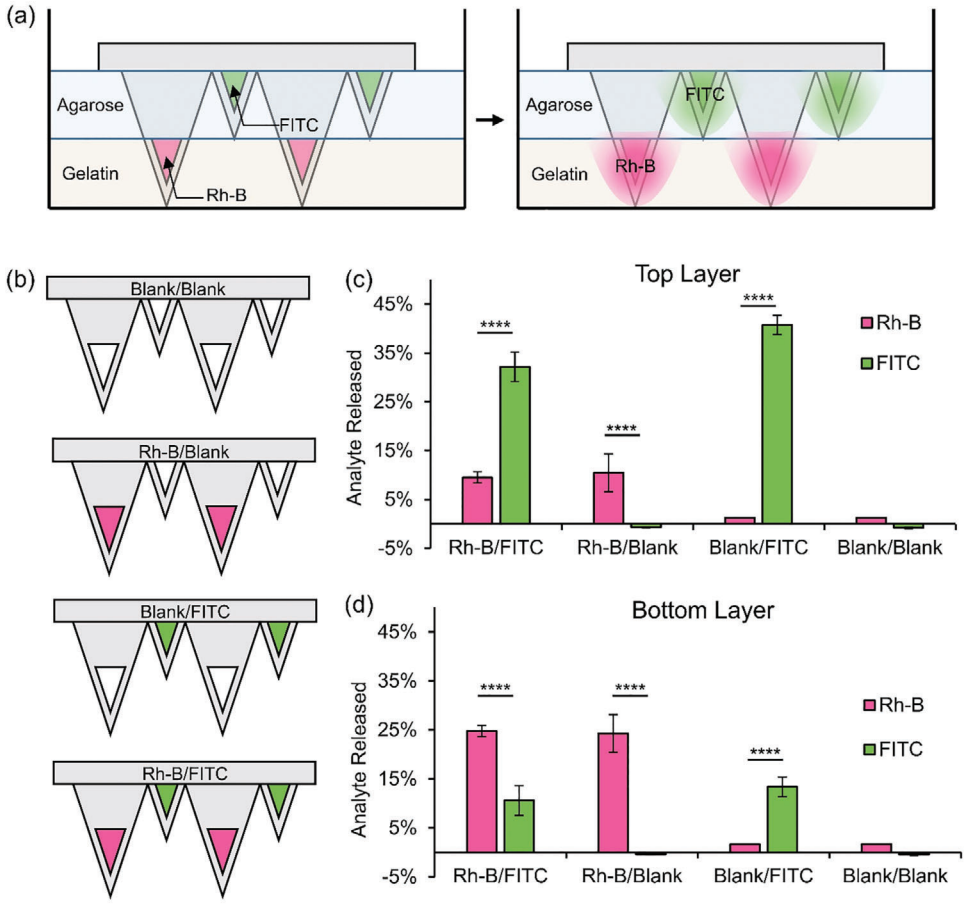

Figure 5. Dual-drug release from multilength MNA. a) Schematic representation of the experimental setup, showing the multilength MNA inserted into the two-gel skin model. b) MNA schematics showing the loading conditions used: both lengths blank, long needles loaded with Rh-B and short needles blank, long needles blank and short needles loaded with BSA–FITC, and long needles loaded with Rh-B and short needles loaded with BSA–FITC. Percent release of Rh-B and BSA–FITC in the c) top, agarose layer and the d) bottom, gelatin layer.

needles. Rather than releasing into phosphate-buffered saline (PBS), these arrays were inserted into a two-gel skin model consisting of agarose and gelatin (**Figure 5**a). Following the release, the gel layers were separated, melted, and read in a plate reader for their Rh-B and BSA–FITC content. The dual release loading, as well as control conditions, are represented schematically in Figure 5b. The measured release results are quantified in Figure 5c. As expected, there is a certain amount of cross contamination between the layers. Like in real skin, there were no barriers between the layers of gel, allowing eventual diffusion of the released molecules from one layer to another. However, the Rh-B signal is stronger in the gelatin, which made up the bottom layer, showing that the longer needles were able to target drug delivery to the desired position. Correspondingly, there is a greater BSA–FITC signal in the top, agarose layer demonstrating the desired release from the shorter needles. This experiment builds on the delivery distribution results seen in Figure 1c,d while emphasizing the versatility of 3D printing to customize MNA designs for different applications.

The ability of the platform to preserve the bioactivity of encapsulated therapeutics was assessed by loading VEGF, an important angiogenic factor. VEGF is known to activate the migration of endothelial cells, and its angiogenic activity was investigated by monitoring the rate of endothelial cell's migration through a standard scratch assay (**Figure 6**). A pipette tip was used to create similarly sized scratches in confluently cultured human umbilical vein endothelial cells (HUVECs), then the treatments were applied. Three different groups were evaluated: MNA − VEGF, MNA + VEGF, and a positive control. In the positive control group, VEGF was mixed with the culture media to induce HUVEC migration and accelerate gap closure.

Although the cytocompatibility of the fabricated structure was confirmed using a Live/Dead assay (Figure S1, Supporting Information), the presence of a needle array resting on the cultured cells may affect their growth. Consequently, VEGF-free MNAs were used as a negative control where the MNAs were placed in the culture media without the incorporation of VEGF in the embedded hydrogel. In the MNA+VEGF group, the needles were filled with 1% (w/v) alginate loaded with VEGF and were similarly placed directly in the well, allowing the VEGF to diffuse into the culture media. Representative images of the scratches for each group are shown for each time point (Figure 6a). As the results show, after 8 h of culture, the MNA+VEGF group exhibited a similar healing potential to the positive control group

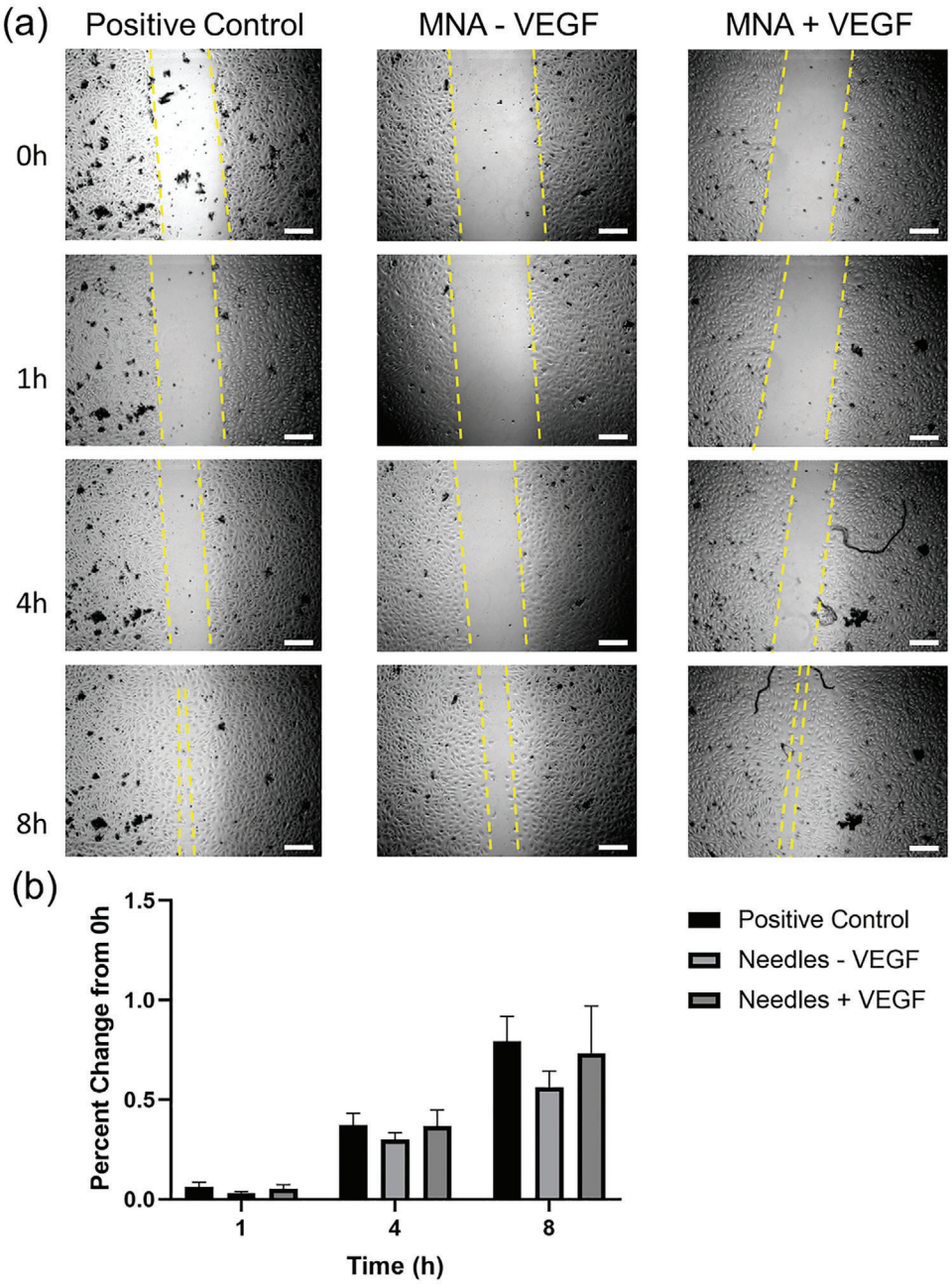

Figure 6. Evaluation of wound healing rate in vitro using scratch assay on cultured HUVECs. a) Qualitative and b) quantitative representation of gap closure in a positive control group where VEGF mixed with the culture media compared to the groups where MNAs without or with the incorporation of VEGF were placed in the culture wells. Scale bars are 250 μm.

where cells nearly closed the gap in its entirety. However, the MNA–VEGF group had a slower healing rate and an observable scratch remained at the end of the study.

Although the differences between the groups were not statistically significant, there is a clear trend in the data (Figure 6b). The healing rate for the MNA+VEGF replicates across all time points was comparable to our positive control, surpassing the MNA–VEGF group. This set of data suggests that VEGF had a positive effect on HUVEC migration. Overall, it can be concluded that the bioactivity of VEGF encapsulated within the gel-filled MNAs was preserved throughout the fabrication and delivery process. Paired with the results seen in Figures 4 and 5, the platform displays the ability to accurately deliver biologically active therapeutics to targeted levels of tissue.

3. Conclusions

In this study, we have developed a robust, customizable, and novel transdermal drug delivery platform. The proposed MNA can be 3D-printed in any desired shape or size and filled with

different hydrogels that encapsulate relevant bioactive factors. The flexibility of the fabrication method in the formation of multilength MNAs provides an opportunity to deliver multiple drugs at different target depths. Looking to the future, use of a more large-scale production method, such as injection molding, and standardization of several sizes and needle configurations may become necessary in order to facilitate commercialization of these MNAs. A rapid filling system was developed to improve the production speed of the platform, as this was the rate-limiting step in complete MNA preparation. The needles withstood compression testing past the force required for skin penetration, and past this value they failed by bending rather than breaking, an optimum failure mode for inserted needles. We have demonstrated their ability to penetrate porcine skin and maintain constituent hydrogels intact during insertion and removal. This allows therapeutics to be removed or replaced easily in a noninvasive fashion if conditions change. The capacity of the platform to be filled with different types of hydrogels and deliver various drug models was successfully demonstrated. Finally, the MNAs were found to be effective at containing and releasing bioactive VEGF and promoting gap closure in an HUVEC scratch assay. Collectively, the developed patch is easy to use and a robust tool for controlling the temporal and spatial distribution of drugs in a passive fashion. Exploration of release kinetics from shorter needles and in animal models should be explored in future work.

4. Experimental Section

Materials: VeroClear RGD810 and TangoBlack FLX973 resins were obtained from Stratasys (MN, USA) and used for 3D printing of MNA dressings. Materials and reagents including NaOH, alginic acid sodium salt, BSA, Irgacure 2959, $CaCl_2$, agarose, ultralow gelling agarose, PEGDA, BSA–FITC, and HUVEC culture media were purchased from Sigma–Aldrich (MO, USA). Other reagents including Human VEGF 165, Dulbecco's PBS (DPBS), fetal bovine serum (FBS), trypsin-ethylenediaminetetraacetic acid (EDTA), Rh-B, and Micro BCA kit were obtained from Thermo Fisher Scientific (MA, USA).

Fabrication of MNAs: The MNAs were designed in SolidWorks (Dassault Systems, France). All arrays were printed using an MJ Stratasys Objet 500 Connex3 3D printer (MN, USA). The needles and the portion of backing directly below them were printed out of VeroClear resin, while the ribs between the islands were printed using TangoBlack simulated rubber material to make the dressing flexible. Support material from the printer was primarily mechanically removed, with the remainder of residues being washed off through soaking in 3% (w/v) NaOH solution suspended in an ultrasonic bath. Prior to being used for the experiments, MNAs were thoroughly rinsed with an ethanol solution (70% v/v) for disinfection and subsequently in DPBS. For the experiments using alginate, loading was performed while MNAs were fully inserted into a 3% (w/v) agarose gel containing 2% (w/v) $CaCl_2$ to crosslink, and in experiments with PEGDA; 30 s of UV exposure was employed for crosslinking the loaded solution containing 1% (w/v) Irgacure 2959 as the photoinitiator. Arrays containing different needle lengths were also similarly printed.

Design and Fabrication of Loading Mechanism: The multineedle filling attachment was designed in SolidWorks with conical channels to mimic the structure of a pipette tip and to facilitate the movement of fluids down and out of the reservoir. It was fabricated using VeroClear with an approach similar to the MNAs. The receiving end of the attachment was designed to fit a P200 micropipette. Following fabrication, the attachment was affixed to a pipette and loaded with the precursor solution, including a 1% (w/v) alginate solution, which was then distributed to each target needle. The solutions were then crosslinked as described before.

Mechanical Characterization of the Engineered MNAs: Mechanical properties of MNAs against compressive mechanical loads were measured using a CellScale Univert Mechanical Tester (ON, Canada). The arrays were affixed to the lower jaw of the tester, the upper jaw was lowered until contact was made, and the mechanical load was applied. A maximum of 200 N compressive force was applied as the jaw was moved at a rate of 0.092 mm s^{-1}.

The penetration capability of MNAs with different compositions was also evaluated using the CellScale Univert Mechanical Tester. The penetration test was performed using three categories of MNAs: all VeroClear arrays, mixed material semiflexible arrays, and arrays fully fabricated on TangoBlack backing all with 3 mm long needles. A 3×3 cm^2 of pig skin was glued to the lower jaw of the tester, and MNAs were glued to the top jaw. The upper jaw was lowered until the tips of the needles were in contact with the pig skin. The compression force was applied as the jaw was moved at a rate of 0.27 mm s^{-1} until the needles were fully penetrated into the skin sample. The samples rested for 1 min before removal at the same rate to measure pull out force.

Hematoxylin and Eosion Staining: Samples of pig skin penetrated with needles were fixed in 10% formalin for 48 h, followed by immersion in 70% ethanol for 24 h. The needles were then retracted, and the samples were cut and embedded in paraffin blocks. The paraffin-embedded skin samples were sectioned into 6 µm thick slices to expose the cross section. Finally, the sections were deparaffinized and stained with H&E. The samples were then inspected using a Zeiss Axio Observer Inverted microscope and images were obtained.

Assessment of Release Kinetics: The potential of the system for the delivery of different drugs encapsulated in various hydrogels at different concentrations was evaluated by assessing the release kinetics of BSA and Rh-B. To perform the release experiments, either BSA or Rh-B was mixed with a hydrogel precursor solution and then loaded into MNAs with eight needles and then crosslinked. For BSA release experiments, 3 mm long needles were filled either with 1% (w/v) alginate or 23% (w/v) PEGDA. The alginate solution was prepared with a stock solution of BSA at a concentration of 2000 µg mL^{-1}, while the PEGDA solution was loaded with 1250 µg mL^{-1} of BSA. MNAs were placed in a 24-well plate. Each well was filled with 0.5 mL of DPBS, and sampling at each time point was performed by removing the entire solution and storing it in a microvial and replacing the sampled volume with fresh DPBS. The BSA content at each time point was assessed with a Micro BCA Protein Assay Kit (Thermo Fisher Scientific), following the manufacturers recommended protocol using a BioTek Cytation 5 plate reader (VT, USA). To compensate for the material interference in the absorbance results, a control group of similar MNAs filled with the same hydrogel, but not carrying any additional molecule, was used. These results were subtracted from the loaded hydrogel release values.

In Rh-B release experiments, solutions of 1%, 2%, and 3% (w/v) sodium alginate were mixed with Rh-B such that complete release would result in a final concentration of 20 µg mL^{-1} in 3 mm long needles. The same solution was loaded into the 2 mm long needles. The MNAs were filled and crosslinked with the same procedures described before. During sampling, only 150 µL of the solution was removed and replaced at each time point. The samples' absorbance values at 560 nm wavelength were read using the BioTek Cytation 5 plate reader. All of the release experiments were performed at least in triplicate.

Evaluation of Dual-Drug Release Capability: For the dual release, MNAs with 4.2 mm long and 2 mm short needles were separately loaded with a 1% (w/v) alginate solution in DPBS containing 46 µg mL^{-1} of Rh-B, 1010 µg mL^{-1} of BSA–FITC, or no added analyte. Four combinations of analyte-loaded alginate MNAs were tested: 1) long needles loaded with Rh-B and short needles loaded with BSA–FITC (Rh-B/FITC); 2) long needles loaded with Rh-B and short needles blank (Rh-B/Blank); 3) long needles blank and short needles loaded with BSA–FITC (Blank/FITC); and (4) both lengths blank (Blank/Blank). The gels were crosslinked as previously mentioned and run in quintuplicate. The needles were inserted into a two-gel skin model that consisted of a 2 mm thick 3% (w/v) ultralow gelling agarose cast on top of a 3 mm thick 10% (w/v) porcine gelatin in 12-well plates. Both solutions were prepared in PBS. A similar gelatin phantom was utilized in existing work in the field.[47] A two-gel model was selected

for this experiment both to simulate multiple distinct layers of skin and to allow for easy separation of the two layers. Ultralow-gelling agarose was selected for the second gel because it is stiff, does not interact with gelatin, and could be melted to take samples. The stiffer agarose gel was cast as the top layer to better mimic the mechanical barrier that the epithelium presents. The initial analyte concentrations loaded into the needles were designed for final concentrations of 20 μg mL^{-1} of FITC–BSA in the top agarose layer and 2 μg mL^{-1} of Rh-B in the bottom gelatin layer. After 16 h, the needles were removed from the two-gel skin. The gels were separated and collected in different containers. The collected gels were melted, and the amount of Rh-B and BSA–FITC was quantified using a BioTek Cytation 5 plate reader at an excitation/emission of 546/568 and 495/520 nm, respectively.

Scanning Electron Microscopy: The microstructures of the alginate hydrogel and gel-filled MNAs were analyzed using SEM. To visualize the porous nature of the alginate, crosslinked alginate hydrogel and gel-filled MNA were immediately frozen in liquid nitrogen. The frozen samples were then lyophilized for 2 days using a Labconco FreeZone Benchtop Freeze Dryer (MO, USA). The crosslinked alginate hydrogel was broken to reveal the internal microstructure. The cross section of the alginate and the filled MNAs were sputtered with palladium using a Cressington 106 Auto Sputter Coater (England, UK). The images were captured using an FEI Quanta 200 Environmental scanning electron microscope (OR, USA) at 10 kV and under a high vacuum.

In Vitro Scratch Assay: HUVECs (Sigma–Aldrich) were cultured in EGM Endothelial Cell Growth Medium BulletKit (Lonza) complete medium. At their fifth passage, the HUVECs were detached using trypsin-EDTA (0.1% w/v), resuspended in the growth medium, and seeded at a concentration of 50 000 cells per well into a 12-well tissue culture plate that was coated with a thin layer of Geltrex hESC-Qualified, Ready-To-Use, Reduced Growth Factor Basement Membrane Matrix (Gibco). The Geltrex layer was formed by diluting by a factor of 2 in the basal endothelial medium and seeding in empty wells. The Geltrex was incubated at 37 °C for 1 h, and then any liquid Geltrex was aspirated. The growth medium was changed every 2 days until the cells became confluent. The cells were starved 12 h before the induction of a scratch by changing the medium to basal medium supplemented with 2% (v/v) fetal bovine serum (Lonza).

A scratch was created in the confluent HUVECs by lightly dragging a P200 pipette tip across the bottom of the well. The medium was changed post scratch to remove any debris and cell fragments from the creation of the scratch. Groups were randomly assigned before determining the initial time point of the scratch. Three groups were assigned and tested ($n = 4$): 1) 1% alginate in MNAs without VEGF (MNA − VEGF), 2) 1% alginate in MNAs with VEGF at a concentration of 6.250 μg mL^{-1} (MNA + VEGF), and 3) positive control with FBS-basal medium supplemented with 50 ng mL^{-1} of human VEGF (Invitrogen). The MNAs were placed in cell culture wells that were prefilled with 2 mL of FBS-basal medium. The concentration of VEGF in the MNA + VEGF group was calculated so that if total VEGF release occurred, the concentration of VEGF in the well would match the concentration of the positive control (50 ng mL^{-1}). Images of the scratches were captured before treatment (0 h) and at various time points after treatment (1, 4, and 8 h). The area of scratch closure for each time point was calculated using ImageJ (NIH, Bethesda, MD) and compared for relative area change to 0 h.

Statistical Analysis: Statistical analysis was performed using GraphPad Prism 8. Values were reported as mean ± standard deviation. All tests were run at least in triplicate. Analysis of variance (ANOVA) was performed for grouped analysis, followed by a Tukey's post-comparison post-test with a p-value of less than or equal to 0.05. p-values of less than 0.05 were considered statistically significant. A p-value of <0.05 was indicated by *, a p-value of <0.01 was indicated by **, a p-value of <0.001 was indicated by ***, and a p-value of <0.0001 was indicated by ****, respectively.

Supporting Information

Supporting Information is available from the Wiley Online Library or from the author.

Acknowledgements

The financial support from the National Institutes of Health (GM126831, AR073822) and the Science and Technology Unit—King Abdulaziz University—Kingdom of Saudi Arabia (Award No. UE-41-106) is gratefully acknowledged.

Conflict of Interest

The authors declare no conflict of interest.

Data Availability Statement

Research data are not shared.

Keywords

chronic wounds, hydrogels, miniaturized needle arrays, wound dressings

Received: November 2, 2020
Revised: April 9, 2021
Published online:

[1] Y.-C. Kim, J.-H. Park, M. R. Prausnitz, *Adv. Drug Delivery Rev.* **2012**, *64*, 1547.
[2] C.-P. Zhou, Y.-L. Liu, H.-L. Wang, P.-X. Zhang, J.-L. Zhang, *Int. J. Pharm.* **2010**, *392*, 127.
[3] L. Daugimont, N. Baron, G. Vandermeulen, N. Pavselj, D. Miklavcic, M.-C. Jullien, G. Cabodevila, L. M. Mir, V. Préat, *J. Membr. Biol.* **2010**, *236*, 117.
[4] Z. Li, Y. He, L. Deng, Z.-R. Zhang, Y. Lin, *J. Mater. Chem. B* **2020**, *8*, 216.
[5] J. Tu, G. Du, M. Reza Nejadnik, J. Mönkäre, K. van der Maaden, P. H. H. Bomans, N. A. J. M. Sommerdijk, B. Slütter, W. Jiskoot, J. A. Bouwstra, A. Kros, *Pharm. Res.* **2017**, *34*, 1693.
[6] a) S. Henry, D. V. McAllister, M. G. Allen, M. R. Prausnitz, *J. Pharm. Sci.* **1998**, *87*, 922;. b) S. Kaushik, A. H. Hord, D. D. Denson, D. V. McAllister, S. Smitra, M. G. Allen, M. R. Prausnitz, *Anesth. Analg.* **2001**, *92*, 502.
[7] a) S. Bystrova, R. Luttge, *Microelectron. Eng.* **2011**, *88*, 1681; b) K. Ita, *J. Drug Delivery Sci. Technol.* **2018**, *44*, 314.
[8] P. M. Wang, M. Cornwell, J. Hill, M. R. Prausnitz, *J. Invest. Dermatol.* **2006**, *126*, 1080.
[9] a) M. Rajabi, N. Roxhed, R. Z. Shafagh, T. Haraldson, A. C. Fischer, W. V. Wijngaart, G. Stemme, F. Niklaus, *PLoS One* **2016**, *11*, e0166330;. b) S. Indermun, R. Luttge, Y. E. Choonara, P. Kumar, L. C. du Toit, G. Modi, V. Pillay, *J. Controlled Release* **2014**, *185*, 130.
[10] a) J. Lim, D. Tahk, J. Yu, D.-H. Min, N. L. Jeon, *Microsyst. Nanoeng.* **2018**, *4*, 29; b) S. J. Moon, S. S. Lee, H. S. Lee, T. H. Kwon, *Microsyst. Technol.* **2005**, *11*, 311.
[11] E. Larrañeta, R. E. M. Lutton, A. D. Woolfson, R. F. Donnelly, *Mater. Sci. Eng., R* **2016**, *104*, 1.
[12] H. S. Gill, M. R. Prausnitz, *Pharm. Res.* **2007**, *24*, 1369.
[13] M. Cormier, B. Johnson, M. Ameri, K. Nyam, L. Libiran, D. D. Zhang, P. Daddona, *J. Controlled Release* **2004**, *97*, 503.
[14] K. Lee, H. C. Lee, D.-S. Lee, H. Jung, *Adv. Mater.* **2010**, *22*, 483.
[15] F. Sammoura, J. Kang, Y.-M. Heo, T. Jung, L. Lin, *Microsyst. Technol.* **2007**, *13*, 517.
[16] Y. Li, H. Zhang, R. Yang, Y. Laffitte, U. Schmill, W. Hu, M. Kaddoura, E. J. M. Blondeel, B. Cui, *Microsyst. Nanoeng.* **2019**, *5*, 41.

[17] W. Martanto, S. P. Davis, N. R. Holiday, J. Wang, H. S. Gill, M. R. Prausnitz, *Pharm. Res.* **2004**, *21*, 947.
[18] D. Han, R. S. Morde, S. Mariani, A. A. La Mattina, E. Vignali, C. Yang, G. Barillaro, H. Lee, *Adv. Funct. Mater.* **2020**, *30*, 1909197.
[19] G. Song, G. Jiang, T. Liu, X. Zhang, Z. Zeng, R. Wang, P. Li, Y. Yang, *ACS Biomater. Sci. Eng.* **2020**, *6*, 4116.
[20] a) Z. Wang, H. Li, J. Wang, Z. Chen, G. Chen, D. Wen, A. Chan, Z. Gu, *Biomaterials* **2020**, *237*, 119782;. b) M. Zheng, Z. Wang, H. Chang, L. Wang, S. W. T. Chew, D. C. S. Lio, M. Cui, L. Liu, B. C. K. Tee, C. Xu, *Adv. Healthcare Mater.* **2020**, *9*, 1901683; c) S. R. Chinnadayyala, I. Park, S. Cho, *Microchim. Acta* **2018**, *185*, 250.
[21] W. Li, R. N. Terry, J. Tang, M. R. Feng, S. P. Schwendeman, M. R. Prausnitz, *Nat. Biomed. Eng.* **2019**, *3*, 220.
[22] a) N. Annabi, A. Tamayol, J. A. Uquillas, M. Akbari, L. E. Bertassoni, C. Cha, G. Camci-Unal, M. R. Dokmeci, N. A. Peppas, A. Khademhosseini, *Adv. Mater.* **2014**, *26*, 85;. b) M. Samandari, F. Alipanah, S. Haghjooy Javanmard, A. Sanati-Nezhad, *Sens. Actuators, B* **2019**, *291*, 418; c) L. J. Eggermont, Z. J. Rogers, T. Colombani, A. Memic, S. A. Bencherif, *Trends Biotechnol.* **2020**, *38*, 418.
[23] a) K. Elkhoury, C. S. Russell, L. Sanchez-Gonzalez, A. Mostafavi, T. J. Williams, C. Kahn, N. A. Peppas, E. Arab-Tehrany, A. Tamayol, *Adv. Healthcare Mater.* **2019**, *8*, 1900506; b) A. Memic, T. Colombani, L. J. Eggermont, M. Rezaeeyazdi, J. Steingold, Z. J. Rogers, K. J. Navare, H. S. Mohammed, S. A. Bencherif, *Adv. Ther.* **2019**, *2*, 1800114; c) P. Villard, M. Rezaeeyazdi, T. Colombani, K. Joshi-Navare, D. Rana, A. Memic, S. A. Bencherif, *Adv. Healthcare Mater.* **2019**, *8*, 1900679.
[24] R. Narayanaswamy, V. P. Torchilin, *Molecules* **2019**, *24*, 603.
[25] J. Li, D. J. Mooney, *Nat. Rev. Mater.* **2016**, *1*, 16071.
[26] a) Y. Qiu, K. Park, *Adv. Drug Delivery Rev.* **2001**, *53*, 321;. b) D. Qureshi, S. K. Nayak, S. Maji, A. Anis, D. Kim, K. Pal, *Eur. Polym. J.* **2019**, *120*, 109220.
[27] a) P. Mostafalu, G. Kiaee, G. Giatsidis, A. Khalilpour, M. Nabavinia, M. R. Dokmeci, S. Sonkusale, D. P. Orgill, A. Tamayol, A. Khademhosseini, *Adv. Funct. Mater.* **2017**, *27*, 1702399; b) S. Bagherifard, A. Tamayol, P. Mostafalu, M. Akbari, M. Comotto, N. Annabi, M. Ghaderi, S. Sonkusale, M. R. Dokmeci, A. Khademhosseini, *Adv. Healthcare Mater.* **2016**, *5*, 175;. c) M. Comotto, S. Saghazadeh, S. Bagherifard, B. Aliakbarian, M. Kazemzadeh-Narbat, F. Sharifi, S. A. Mousavi Shaegh, E. Arab-Tehrany, N. Annabi, P. Perego, A. Khademhosseini, A. Tamayol, *J. Biomater. Appl.* **2019**, *33*, 1265.
[28] R. Dimatteo, N. J. Darling, T. Segura, *Adv. Drug Delivery Rev.* **2018**, *127*, 167.
[29] K. Lee, Y. Xue, J. Lee, H.-J. Kim, Y. Liu, P. Tebon, E. Sarikhani, W. Sun, S. Zhang, R. Haghniaz, B. Çelebi-Saltik, X. Zhou, S. Ostrovidov, S. Ahadian, N. Ashammakhi, M. R. Dokmeci, A. Khademhosseini, *Adv. Funct. Mater.* **2020**, *30*, 2000086.
[30] a) Z. Luo, W. Sun, J. Fang, K. Lee, S. Li, Z. Gu, M. R. Dokmeci, A. Khademhosseini, *Adv. Healthcare Mater.* **2019**, *8*, 1801054; b) X. Zhou, Z. Luo, A. Baidya, H.-j. Kim, C. Wang, X. Jiang, M. Qu, J. Zhu, L. Ren, F. Vajhadin, P. Tebon, N. Zhang, Y. Xue, Y. Feng, C. Xue, Y. Chen, K. Lee, J. Lee, S. Zhang, C. Xu, N. Ashammakhi, S. Ahadian, M. R. Dokmeci, Z. Gu, W. Sun, A. Khademhosseini, *Adv. Healthcare Mater.* **2020**, *9*, 2000527.
[31] a) C. P. P. Pere, S. N. Economidou, G. Lall, C. Ziraud, J. S. Boateng, B. D. Alexander, D. A. Lamprou, D. Douroumis, *Int. J. Pharm.* **2018**, *544*, 425;. b) M. A. Luzuriaga, D. R. Berry, J. C. Reagan, R. A. Smaldone, J. J. Gassensmith, *Lab Chip* **2018**, *18*, 1223;. c) H. Derakhshandeh, F. Aghabaglou, A. McCarthy, A. Mostafavi, C. Wiseman, Z. Bonick, I. Ghanavati, S. Harris, C. Kreikemeier-Bower, S. M. Moosavi Basri, *Adv. Funct. Mater.* **2020**, *30*, 1905544.
[32] A. R. Johnson, C. L. Caudill, J. R. Tumbleston, C. J. Bloomquist, K. A. Moga, A. Ermoshkin, D. Shirvanyants, S. J. Mecham, J. C. Luft, J. M. DeSimone, *PLoS One* **2016**, *11*, e0162518.
[33] K. Lee, E. A. Silva, D. J. Mooney, *J. R. Soc., Interface* **2011**, *8*, 153.
[34] Y. Shoham, Y. Krieger, E. Tamir, E. Silberstein, A. Bogdanov-Berezovsky, J. Haik, L. Rosenberg, *Int. Wound J.* **2018**, *15*, 769.
[35] L. Barnum, M. Samandari, T. A. Schmidt, A. Tamayol, *Expert Opin. Drug Delivery* **2020**, *17*, 1767.
[36] P. A. J. Kolarsick, M. A. Kolarsick, C. Goodwin, *J. Dermatol. Nurses Assoc.* **2011**, *3*, 203.
[37] M. Venus, J. Waterman, I. McNab, *Surgery* **2010**, *28*, 469.
[38] M. Samandari, F. Aghabaglou, K. Nuutila, H. Derakhshandeh, Y. Zhang, Y. Endo, S. Harris, L. Barnum, C. Kreikemeier-Bower, E. Arab-Tehrany, N. A. Peppas, I. Sinha, A. Tamayol, *Adv. Healthcare Mater.* **2021**, *10*, 2001800.
[39] a) P. Bao, A. Kodra, M. Tomic-Canic, M. S. Golinko, H. P. Ehrlich, H. Brem, *J. Surg. Res.* **2009**, *153*, 347;. b) Y.-K. Hong, B. Lange-Asschenfeldt, P. Velasco, S. Hirakawa, R. Kunstfeld, L. F. Brown, P. Bohlen, D. R. Senger, M. Detmar, *FASEB J.* **2004**, *18*, 1111.
[40] H. Rossiter, C. Barresi, J. Pammer, M. Rendl, J. Haigh, E. F. Wagner, E. Tschachler, *Cancer Res.* **2004**, *64*, 3508.
[41] H. Derakhshandeh, S. S. Kashaf, F. Aghabaglou, I. O. Ghanavati, A. Tamayol, *Trends Biotechnol.* **2018**, *36*, 1259.
[42] a) T. D. Ngo, A. Kashani, G. Imbalzano, K. T. Nguyen, D. Hui, *Composites, Part B* **2018**, *143*, 172; b) H. N. Chia, B. M. Wu, *J. Biol. Eng.* **2015**, *9*, 4.
[43] N. Faramarzi, I. K. Yazdi, M. Nabavinia, A. Gemma, A. Fanelli, A. Caizzone, L. M. Ptaszek, I. Sinha, A. Khademhosseini, J. N. Ruskin, A. Tamayol, *Adv. Healthcare Mater.* **2018**, *7*, 1701347.
[44] A. Sood, M. S. Granick, N. L. Tomaselli, *Adv Wound Care* **2014**, *3*, 511.
[45] Y. Niu, Q. Li, Y. Ding, L. Dong, C. Wang, *Adv. Drug Delivery Rev.* **2019**, *146*, 190.
[46] Y. Zhao, F. Li, M. T. Carvajal, M. T. Harris, *J. Colloid Interface Sci.* **2009**, *332*, 345.
[47] T. Yilmaz, R. Foster, Y. Hao, *IEEE Trans. Antennas Propag.* **2014**, *62*, 3064.